Amirkabir University of Technology
(Tehran Polytechnic)

An experimental investigation on the effects of attaching winglets

Course instructor:

Dr. M. Mani

Teacher assistant:

Mr. Kazemi

Groupe Number 2

Winter 2020

Contents

List of Figures

Introduction

Thin airfoil theory was developed in Germany throughout ward war II. It is far away from the only tractable means of obtaining analytical solutions for lift and moments on an airfoil. However, thin airfoil theory holds just for thin airfoils at little angles of attack. However, this can be not as restrictive as it seems as a result of several airplanes over the past years have comparatively thin airfoils and cruise at comparatively little angles of attack.

Since the 1960s, the arrival and development of the high-speed computer allowed elaborate numerical solutions supported the circulation theory of carrying, solutions for the carry on a body of arbitrary form and thickness at any angle of attack.

A device section, an essential part of a wing, has its primary task as a carry generator. The correct functioning of the device is the necessity of the satisfactory performance of the lifting surface. An airfoil formed body is enraptured through a fluid that produces aerodynamic forces. The part of force perpendicular to the direction of motion is termed lift. The element parallel to the direction of movement is termed Drag. The lift made is primarily the result of its Angle of Attack and shape. When directed at a proper angle, the airfoil deflects the oncoming air leading to a force on the

airfoil within the direction opposite to the deflection. This force is thought of as force and might be resolved into two components lift and Drag.

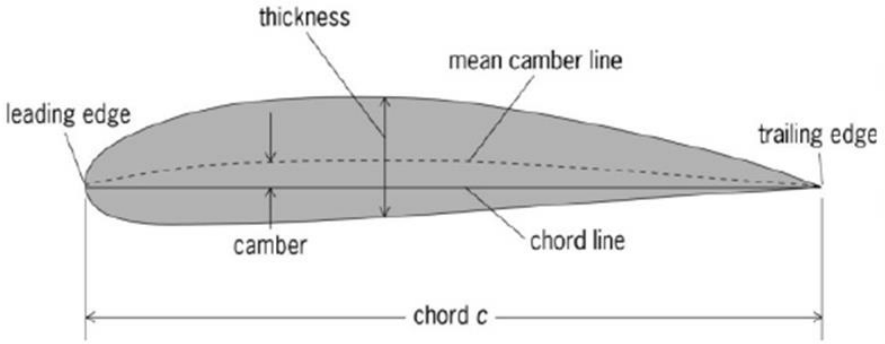

Figure 1- An airfoil section

2D airfoil theory

The basic equations necessary for calculating airfoil lift and moments with an application to symmetric airfoils and dealing with thin airfoils are first essential knowledge in aerodynamics; for such a case, the airfoil is often simulated by a vortex sheet placed on the camber line. The purpose is to calculate the variation of $\gamma(s)$ such that the camber line becomes a streamline of the flow and such that the Kutta condition is satisfied at the trailing edge; that is, $\gamma(TE) = 0$. Once we have found the particular $\gamma(s)$ that satisfies these conditions, then the total circulation around the airfoil is found by integrating $\gamma(s)$from the leading edge to the trailing edge. In turn, the lift is calculated via the Kutta-Joukowski theorem. Kutta-Joukowski theorem says that for a closed two-dimensional body of arbitrary shape, the lift per unit span is $L=\rho_\infty V_\infty \Gamma$.

The airfoil as infinite wing Vs. Finite wing

A finite wing could be a three-dimensional body, and consequently, the flow over the finite wing is three-dimensional; there's an element of flow within the spanwise direction.

The physical mechanism for generating lift on the wing is the existence of a high on the bottom surface and low pressure on the top surface. the net imbalance of the pressure distribution creates the lift. As a by-product of this pressure imbalance, the flow close to the wingtips tends to twist round the tips, being forced from the high-pressure region only beneath the guidelines to the low-pressure area on top. This flow around the wingtips is shown within the front view of the wing. As a result, on the wing's top surface, there's usually a spanwise element of flow from the tip toward the wing root, causing the streamlines over the top surface to bend toward the root. On the wing's bottom surface, there's usually a spanwise element of ensuing the foundation toward the tip, inflicting the streamlines over the bottom surface to bend toward the tip. The flow over the finite wing is three-dimensional, and therefore it might be expected the aerodynamic properties of such a wing to differ from those of its airfoil sections.

The tendency for the flow to “leak” around the wingtips has another vital result on the wing's aeromechanics. This flow establishes a circulatory motion that trails downstream of the wing; that's, a trailing vortex is made at each wingtip.

The aerodynamics of finite wings is analyzed victimization the classical lifting line model. This easy model permits a closed-form resolution that captures most of the physical effects applicable

to finite wings. The model is based on the horseshoe-shaped vortex that introduces the conception of a vortex wake and wingtip vortices. The downwash elicited by the wake creates an induced drag that didn't exist within the two-dimensional analysis.

Important Aerodynamic Basics
The Boundary Layer

The friction of the air on the walls of a body around that it circulates slows down the flow among a thin layer adhering to the walls. This layer is thought of as a "boundary layer. “

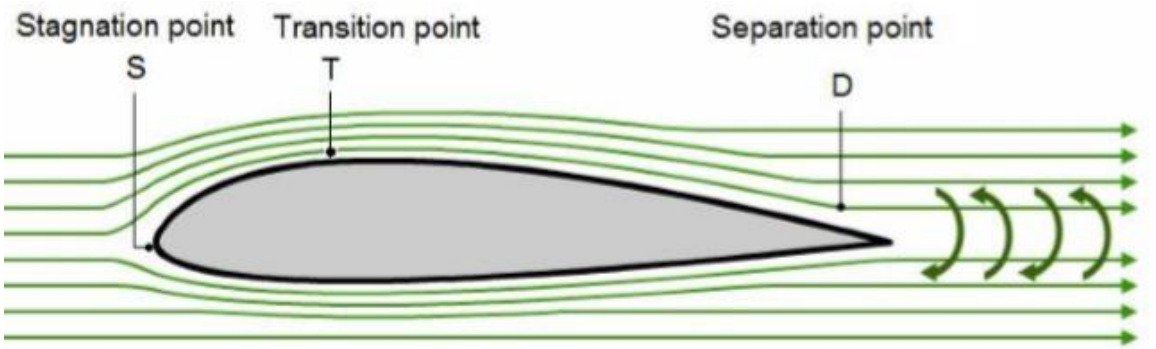

Figure 2- Airflow over an airfoil

The boundary layer's existence is because of the consistency of the air, which isn't an ideal gas. Throughout the flow, some molecules travel on the side and others on the lower surface of the body, and therefore the following ways area unit obtained delimited by:

- **The stagnation purpose (S):**

The boundary layer exists as soon as there's a flow. It begins at the stagnation purpose "A" on the side similar to the lower surface, and the flow is at the first laminar. Within the stagnation purpose, the overall pressure is exerted. It's a high-pressure area.

- **The transition purpose (T):**

At some extent, “T” called the “transition point,” the flow becomes turbulent. The boundary layers from the higher and lower surface meet at the edge and type the wake

- **The separation purpose (D):**

The flow changes from the transition purpose T; the airflows don't seem to be parallel any longer and flow in a very disordered manner. This alteration corresponds to a little increase in the thickness of the boundary layer. Flow, therefore, starts from the transition purpose to the separation purpose “D.”

Boundary-Layer

The boundary layer's existence was discovered by noting that fine dust which was on the wings of a plane did not disappear in flight or raindrops move slowly on the walls of the airframe. The boundary layer starts from the stagnation point to the trailing edge with a variation in thickness of about a few millimeters to a few centimeters. In this thin layer, very significant forces of viscosity

are present, as well as large speed variations when moving away perpendicularly from the skin. Conventionally the boundary layer thickness is defined by the distance on the wall from which the rate of flow is equal to $v = 0.99\ v_0$ (v_0 being the infinite speed at the normal of the skin).

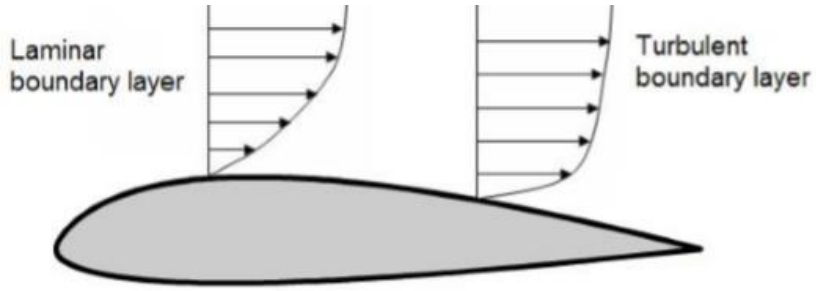

Figure 3- Laminar and Turbulent Boundary Layer

Laminar and Turbulent Flow
Laminar flow:

The initial flow of the boundary layer is laminar. It is located between the stagnation point and the transition point. Within the boundary layer, the airflows are parallel and slide over one another. If we look at the flight path vectors of a laminar layer, it is seen that they go from a value equal to zero to a value close to the rate of flow. All these vectors are parallel to one another.

Turbulent flow:

The flow changes from the transition point T; the airflows are no longer parallel and flow in a disordered manner. This change corresponds to a small increase in the thickness of the boundary layer. Turbulent flow thus starts from the transition point to the separation point "D." At the separation point, the boundary starts to detach, the particles close to the skin have their movement reversed, thus causing the formation of vortices (resulting in a significant increase in Drag).

Free Stream Flow

A flow is taken into account to be steady if its properties in each purpose have no modification with time. Let us consider an ideal fluid: If the molecules of the fluid do not exert any friction between them or the skin of the body, i.e., there is a complete absence of friction, and that the volume of the fluid, independent of its size, is not affected in its movement, the flow is considered to be steady. Change within the flow to time: The pressure P and speed v at an equivalent point vary continuously in an exceedingly disorderly manner. The flow is "unsteady. " These types of flow in aerodynamics will be avoided. They give rise to energy dissipations (vortices). Generally, a particle can have three types of movement: rotation, translation, and deformation. When there is no rotational movement of the particles, it is said that the flow is laminar. When there is a rotation of the fluid particles, it is said that there is a vortex.

Relative Airflow

Relative airflow could be a term used to describe the flow's direction with relation to the wing. In other texts, it's typically referred to as relative wind. If a wing is moving forward and downward, the relative airflow is upward and backward. If the wing is moving forward horizontally, the

relative airflow moves backward horizontally. The flight path and the relative flow are, therefore, invariably parallel. However, travel in opposite directions. The motion makes relative airflow of the airplane through the air. It's conjointly created by the motion of air past a stationary body or by a mix of both. Therefore, on a takeoff roll, a plane is subject to the relative airflow created by its motion on the bottom and conjointly by the moving mass of air (wind). In-flight, however, solely the motion of the plane produces a relative airflow. The direction and speed of the wind don't have any impact on relative airflow.

Finite Wing Effects

Speed can be calculated in magnitude and direction at all external points of the airfoil. Vortices are formed when the boundary layer separates from the airfoil. These vortices cause a change in speed in the flow known as designated speed "ω." Aerodynamic deflection at a point is the angle "ε" formed by the rate of the flow with infinite upstream speed.

Wingtip Vortices

Wingtip vortices are tubes of circulating air that is left behind by the wing as it generates lift. Each wingtip vortex starts from the tip of each wing. The cores of vortices spin at very high speed, and they are regions of very low pressure. The cores of wingtip vortices are sometimes visible because of water vapor's condensation at very low pressure.

Wingtip vortices are related to induced Drag, an essentially unavoidable side-effect of the wing generating lift. Managing induced drag and wingtip vortices and choosing the best wing planform for the mission is critically vital in aerospace engineering. Wingtip vortices form the major elements of wake turbulence.

Figure 4- the picture is from Van Dyke's Album of Fluid Motion depicts low-speed flow over a lifting wing of finite span.

Figure 5- Vortex side view (Van Dyke's Album of Fluid Motion)

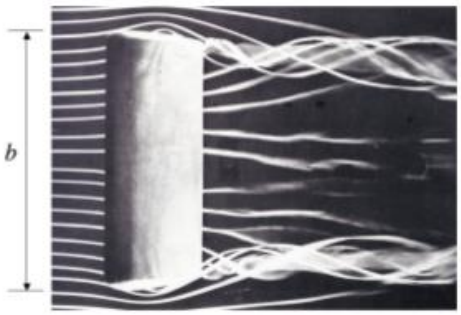

Figure 6- Vortex top view (Van Dyke's Album of Fluid Motion)

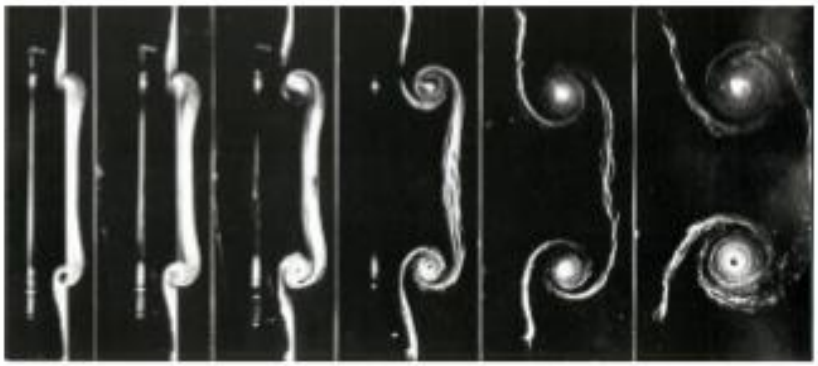

Figure 7- Vortices back view (Van Dyke's Album of Fluid Motion)

These pictures seriously illustrate the three-dimensional flow over the wing. In every case, the wing has lift resulting in reduced pressure above the wing and exaggerated pressure below the free stream pressure.

The upstream influence of the elevated pressure below the wing leads to a divergence of the smoke lines before the wing. If the smoke lines had been positioned to pass above the wing, one would instead see a convergence driven by the suction surface's low pressure. This vital impact can even

be seen within the smoke lines that leave the wingtips' trailing edge and diverge outward to affix the wingtips' vortex rollup.

Near the wing, the bound circulation ends up in an up-wash before the wing and downwash behind the wing, similar to the flow created by a two-dimensional lifting wing of infinite span.

The flow generates a very vital impact because of the vortex combination that contains the wake. The semi-infinite sheet of vorticity distributed within the wake produces a downward velocity element within the free-stream before the wing, at the wing, and far downstream.

The downwash by the wake results in a discount within the wing's angle-of-attack relative to the free stream, reducing the lift. Additionally, the downwash rotates the oncoming flow vector at the wing resulting in an element of Drag. And this can be the results, added in real finite wings aerodynamic characteristics. CFD simulations have shown this phenomenon, and here the results of one simulation are according. These results are valid with National Aeronautics and Space Administration experimental works. They show pressure coefficient contours at vortex for various locations(x/c), computed at 10° angle of attack and free stream velocity of 170 ft/s.

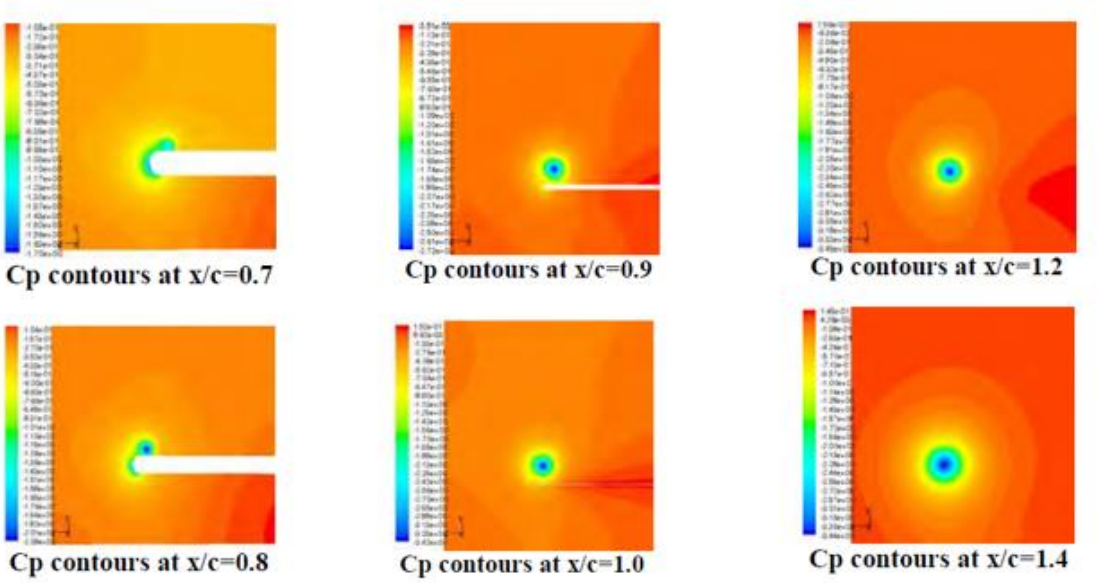

Figure 8- Cp contours at a different location (looking upstream from the back)

If an airfoil's vortex produces downwash in different places, the airframe should conjointly manufacture an identical quantity of upwash; in "stable flight," this happens more or less within the frame surface envelope; it can conjointly occur outside of the airframe envelope below special circumstances. The term upwash is used to visit regions around a craft or airfoil wherever the air is acquiring the alternative direction to downwash. The wingtip vortices induce an upwash outside the wingspan of a craft or airfoil equalization downwash created by upper wing surfaces. Migratory birds build use of this upwash when they fly in an exceedingly V formation.

Methods Candidate to Use

Surface Pressure Distributions

The pressure distributions of both upper and lower surfaces along the chord length of four segments (Segment- A, B, C, and D) is being chosen for four experimental wing models at the selected angle of attack (AOA). From the static pressure data, the respective coefficient of pressure (C_p) is calculated using equations, which are discussed in this part.

The wind tunnel has a reference pressure tap located upstream of the test section, and the pressure there is calculated from the equation below

Values of Cp at any point over the airfoil surface can be approximated from the corresponding boundary values by using the first order Lagrange interpolation and extrapolation:

$$P_\infty = \rho_{water} g (h_{atm} - h_\infty) \quad \text{(Eq. 01)}$$

$$C_p(x) = \frac{(x - x_1)}{(x_0 - x_1)} C_{P,0} - \frac{(x - x_0)}{(x_1 - x_0)} C_{P,1} \quad \text{(Eq. 02)}$$

the results will be shown in a figure in which the horizontal axis represents the chord length percentage (%C). The vertical axis represents the surface pressure coefficient (C_p). The vertical axis above the zero lines (horizontal axis) denotes the negative pressure coefficients or suction pressure coefficients. The vertical axis below the zero lines denotes the positive pressure coefficients. The pressure coefficients of a wing without a winglet are also measured and plotted. Then the surface pressure distribution of all the wing planforms is discussed and compared.

Lift Characteristics

The data taken from the pressure distribution are accustomed to calculate traditional and axial forces on the wing models from balance. These traditions are employed to work out the constant of elevating (CL). Then the impact of the angle of attack on CL is studied and employed in comparison.

The lift will increase with an increase in the angle of attack to a maximum value. Maximum this most value of attack angle, elevate decreases drastically thanks to flow separation over the device surface. The elevate coefficients of the wing models underneath check for the various angle of attack (AOA). This half has illustrated the comparison of the values of elevating constant for wings and the stall angle of attack.

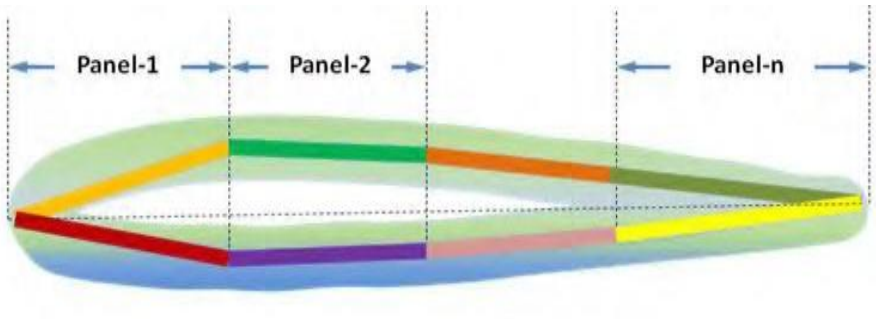

Figure 9- Paneling of the Wing Surface

Both the wing section surfaces can be divided into small panels corresponding to a total of gaps between each pressure tap location. When n is several panels, the equations can be converted to:

$$C_n = \sum_{i=1}^{n} [(c_{p,l,i} - c_{p,u,i})\Delta(\frac{x_i}{c})] \quad \text{(Eq. 03)}$$

$$C_a = \sum_{i=1}^{n} [(c_{p,u,i}\frac{\Delta_{y_{u,i}}}{\Delta_{x_i}} - c_{p,u,i}\frac{\Delta_{y_{l,i}}}{\Delta_{x_i}})\Delta(\frac{x_i}{c})] \quad \text{(Eq. 04)}$$

The interpolated and extrapolated pressure coefficients would be applied to Equation to get the normal and axial force at a section of interest. Lift and drag coefficient can be obtained from:

$$C_l = C_n Cos\alpha - C_a Sin\alpha \quad \text{(Eq. 05)}$$

Drag Characteristics

The data taken from the pressure distribution are used to calculate normal and axial forces on the wing models. These axials are used to determine the coefficient of drag (C_D). Then the effect of angle of attack on C_D is studied and used in the comparison. The drag coefficients of the wing models under test for a different angle of attack (AOA). This part has illustrated the comparison of the drag coefficient values for wings and the critical angle of attack within the drag coefficient rise.

Besides considering all equation in the lift part, the drag coefficient is calculated from the equation below:

$$C_d = C_n Sin\alpha + C_a Cos\alpha \quad \text{(Eq. 06)}$$

Lift to Drag Ratio

The data taken from the pressure distribution are used to calculate normal and axial forces on the wing models. These normal and axial forces are used to determine the coefficient of lift (C_L), coefficient of drag (C_d), and lift to drag ratio (L/D) of an individual wing. Then the effect of angle of attack on C_L, C_D, and L/D is studied and used in the comparison.

The values of lift to drag ratio are plotted for various angles of attack. From this graph, it is observed that the lift to drag ratio for wing with two wing models and. It is also evident that the wing without winglet has the lowest lift to drag ratio compared to wing with winglet models. It can also be found that the lift to drag ratio pattern is a similar trend with National Airfoil Data selected NACA or not.

Induced Drag

Induced drag coefficients CD, I of all wing models are calculated from the value of CL at a respective angle of attack from the equation below:

$$C_{D,i} = \frac{C_l^2}{\pi e AR} \quad \text{(Eq. 07)}$$

The wing models' induced drag coefficients were under test for different angles of attack (AOA). It must be observed that the induced drag for a wing without winglets is greater than a wing with winglets. From the plot and also data, the two-winglet model and also wing without winglet will be compromised.

Experimental Setup

The experiments done for this investigation on the effects of adding winglets were conducted in the low-speed, open-return wind tunnel in DANA Aerodynamics Laboratory. This tunnel has a test section with a length of 1.8m and a cross-section of 1 × 1 m with air velocity, adjustable between 5 and 60 m/s at the turbulence intensity of approximately 25 %. The model was mounted on a three-component aerodynamic balance of model TE44 to measure lift and drag forces. The Aluminum alloy balance consists of a fixed plane to the wall of the tunnel's test section, and a triangular plane is attached to this plane. The model is mounted on the plane inside the test section, and the triangular plane is connected to the plane inside by three supporting arms. Each arm is connected to the triangular plane and the attachment plane by spherical junctions, so in this way, the plane which is directly experiencing the forces is limited in moving in its plane, parallel with the triangular plane but can rotate freely around an axial shaft where the model is seated. This methodology brings us with the forces in three directions.

The test was done three times, first on the plane 3D wing without winglet and then for two modes: adding a half winglet and the doubled winglet of the same type. These two winglets were attached to the tip of the wing to investigate their influential characteristics on the lift and drag of the wing. The experiments were performed separately at constant wind velocity set at 15 m/s and the change in the angle of attack from -4 degrees to +20 degrees for each model.

Table 1- Dimensional Data

component	parameter	value
Wing	Area, m^2	0.06
	Span, m	0.30
	Mean aerodynamic chord, m	0.05
	wing root & tip chord, m	0.20

Results, Discussion, and Conclusion

The results are presented in the order of tests, reviewed in the previous chapter, first for the clean strategy, second for the model with half-winglet added, and third for the doubled-winglet added. Based on the air density of 1.2 Kg/m^3 and U= 15 m/s, the Reynolds number is 2.44×10^5.

Clean Wing

Table 2- Clean Wing data

Clean	CL	CD
offset	0.000	0.000
-4	-0.011	0.020
-2	-0.021	0.079
0	0.000	0.062
2	0.019	0.046
4	0.019	0.052
6	0.041	0.033
8	0.052	0.026
10	0.109	0.056
12	0.104	0.082
14	0.139	0.092
16	0.169	0.079
18	0.161	0.098
20	0.199	0.151

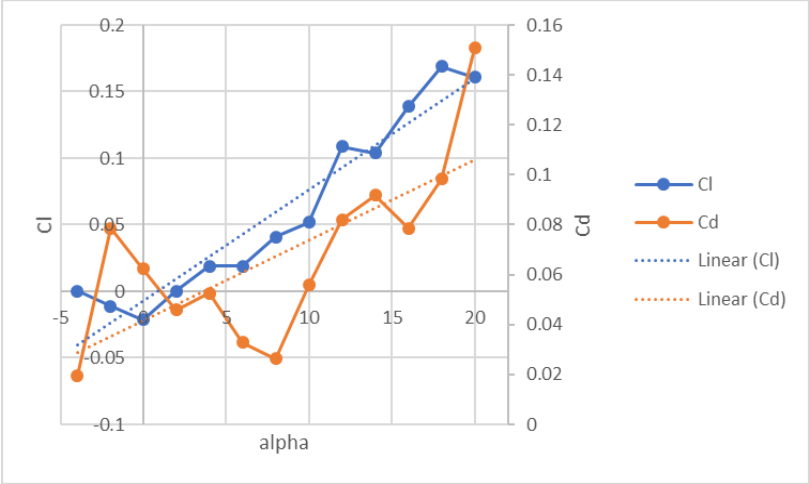

Figure 10- clean wing plotted data

Figure 11- Clean Wing

Wing with one-sided winglet

Table 3- wing with one-sided winglet data

Clean	CL	CD
offset	0	0
-4	0.019	0.016
-2	0.112	0.030
0	0.130	0.056
2	0.160	0.056
4	0.179	0.056
6	0.182	0.056
8	0.220	0.082
10	0.223	0.069
12	0.269	0.102
14	0.280	0.128
16	0.272	0.148
18	0.318	0.193
20	0.337	0.200

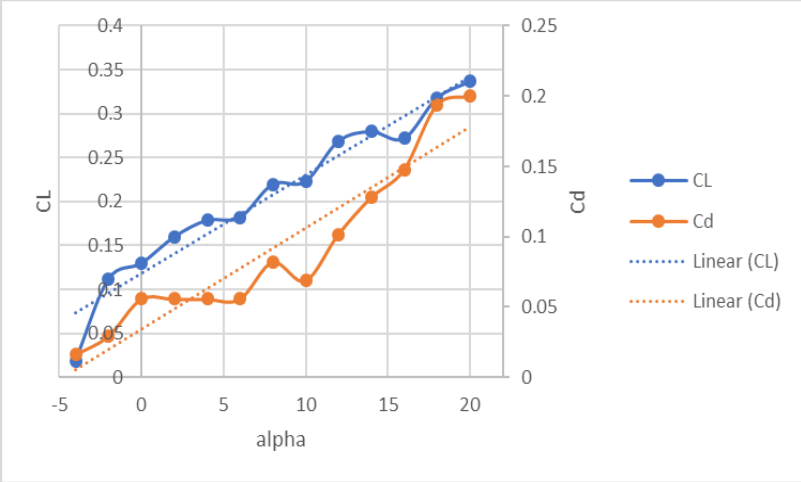

Figure 13- one-sided winglet plotted data

Figure 12-one-sided winglet

The experiment is done with the wing shown in Figures 4 and 5 with a winglet added at its root. As expected, the lift coefficient grows with the AOA increase by one degree per each step. It is also seen that the drag coefficient increases with the increase in AOA. The winglet shown is a triangle-type winglet and one-sided and is expected to increase the lift coefficient but reduce the drug-induced coefficient.

Figure 14- wing with one-sided winglet

Wing with double-sided winglet

Table 4- wing with double-sided wing

Clean	CL	CD
offset	0.000	0.000
-4	0.000	0.033
-2	0.065	0.043
0	0.095	0.033
2	0.133	0.046
4	0.155	0.020
6	0.193	0.052
8	0.204	0.066
10	0.207	0.059
12	0.253	0.089
14	0.264	0.111
16	0.283	0.131
18	0.313	0.171
20	0.302	0.197

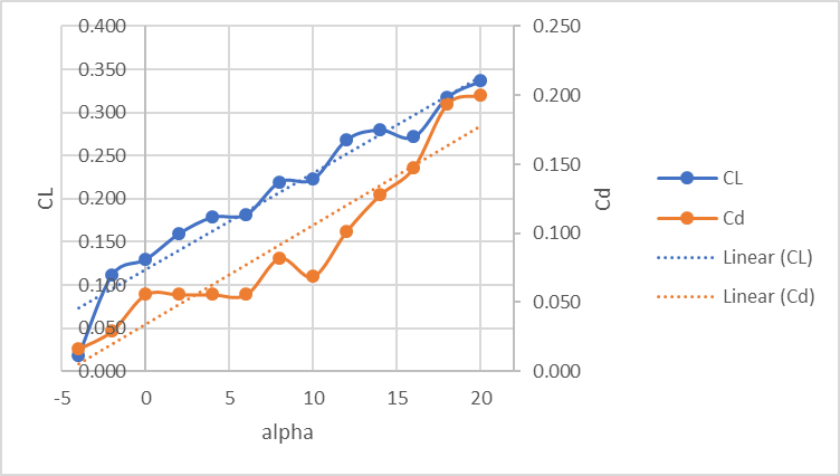

Figure 15- double-sided winglet plotted data

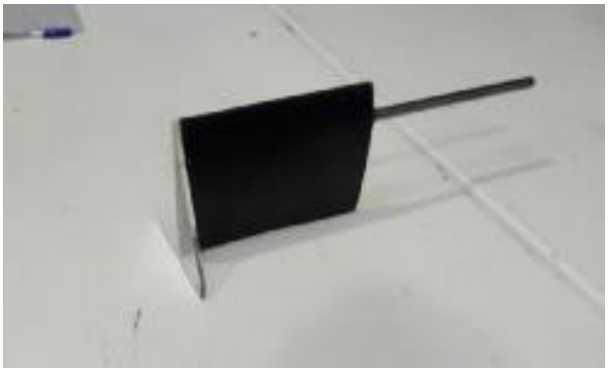

Figure 16-wing with double-sided winglet

The second experiment on a wing with a winglet included is done with a triangle-type but double-sided winglet. This winglet is also expected to increase the lift coefficient and reduce the drag coefficient by decreasing the tip vortices at the wing's tip to reduce induced drag.

Figure 17-double-sided winglet

Comparison and discussion

Table 5 - all data comparison

Alpha	Clean			W1			W5		
	Cl	CD	Cl/Cd	Cl2	CD2	Cl/Cd2	Cl4	CD5	Cl/Cd5
offset	0.000	0.100	0.000	0.000	0.100	0.000	0.000	0.100	0.000
-4	-0.011	0.020	-0.559	0.019	0.016	1.157	0.000	0.033	0.000
-2	-0.021	0.079	-0.273	0.112	0.030	3.793	0.065	0.043	1.522
0	0.000	0.062	0.000	0.130	0.056	2.328	0.095	0.033	2.893
2	0.019	0.046	0.413	0.160	0.056	2.866	0.133	0.046	2.893
4	0.019	0.052	0.362	0.179	0.056	3.207	0.155	0.049	3.148
6	0.041	0.033	1.250	0.182	0.056	3.261	0.193	0.052	3.675
8	0.052	0.026	1.982	0.220	0.082	2.680	0.204	0.066	3.107
10	0.109	0.056	1.954	0.223	0.069	3.235	0.207	0.059	3.504
12	0.104	0.082	1.268	0.269	0.102	2.643	0.253	0.089	2.855
14	0.139	0.092	1.513	0.280	0.128	2.187	0.264	0.111	2.366
16	0.169	0.079	2.146	0.272	0.148	1.841	0.283	0.131	2.156
18	0.161	0.098	1.636	0.318	0.193	1.642	0.313	0.171	1.834
20	0.199	0.151	1.318	0.337	0.200	1.683	0.302	0.197	1.533

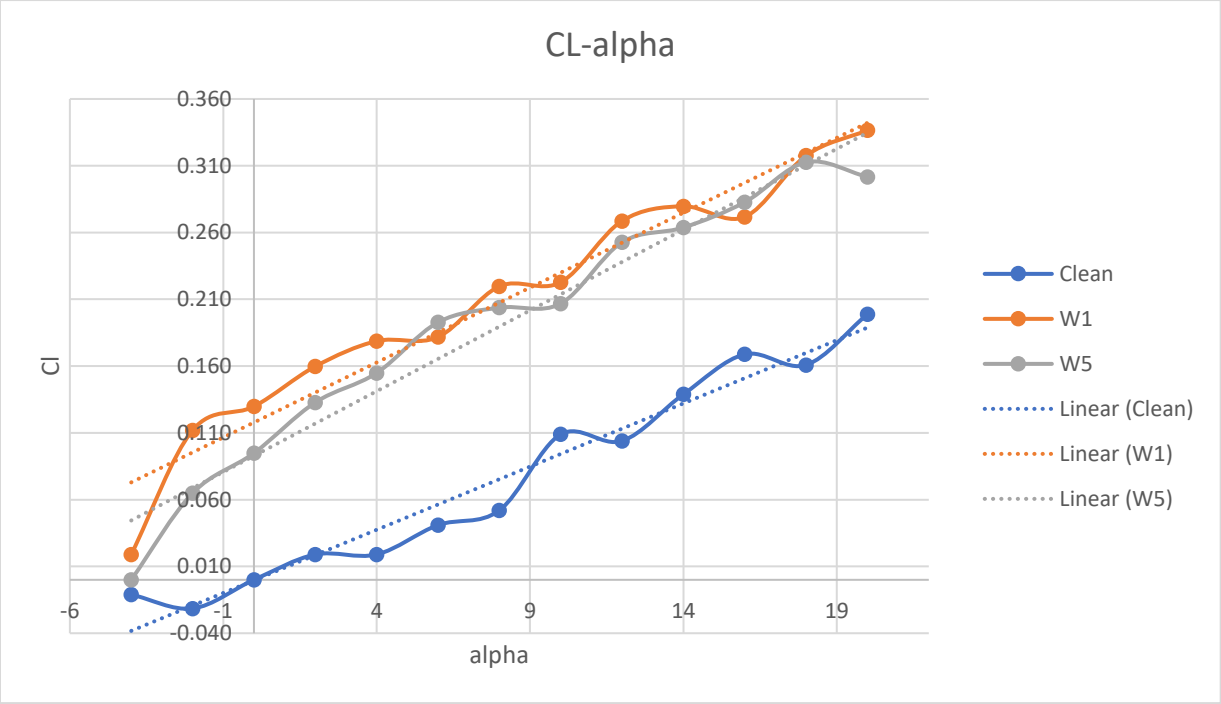

Figure 18- Cl-alpha comparison

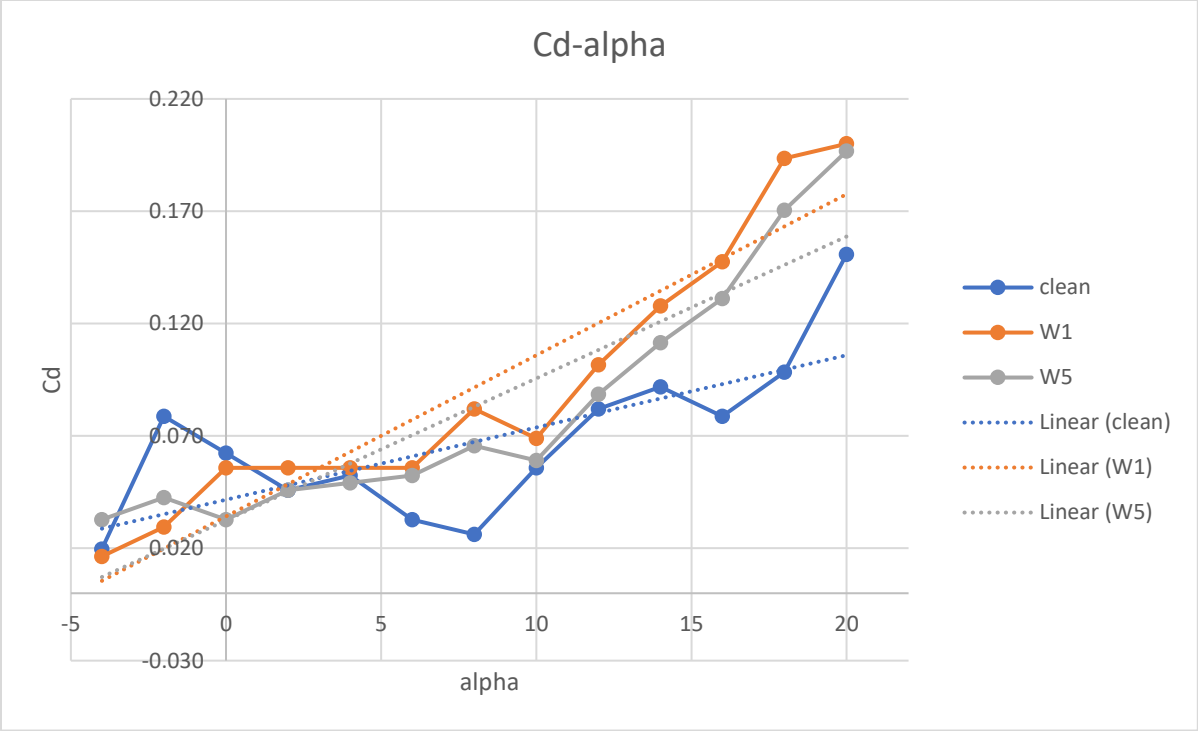

Figure 19-- Cd-alpha comparison

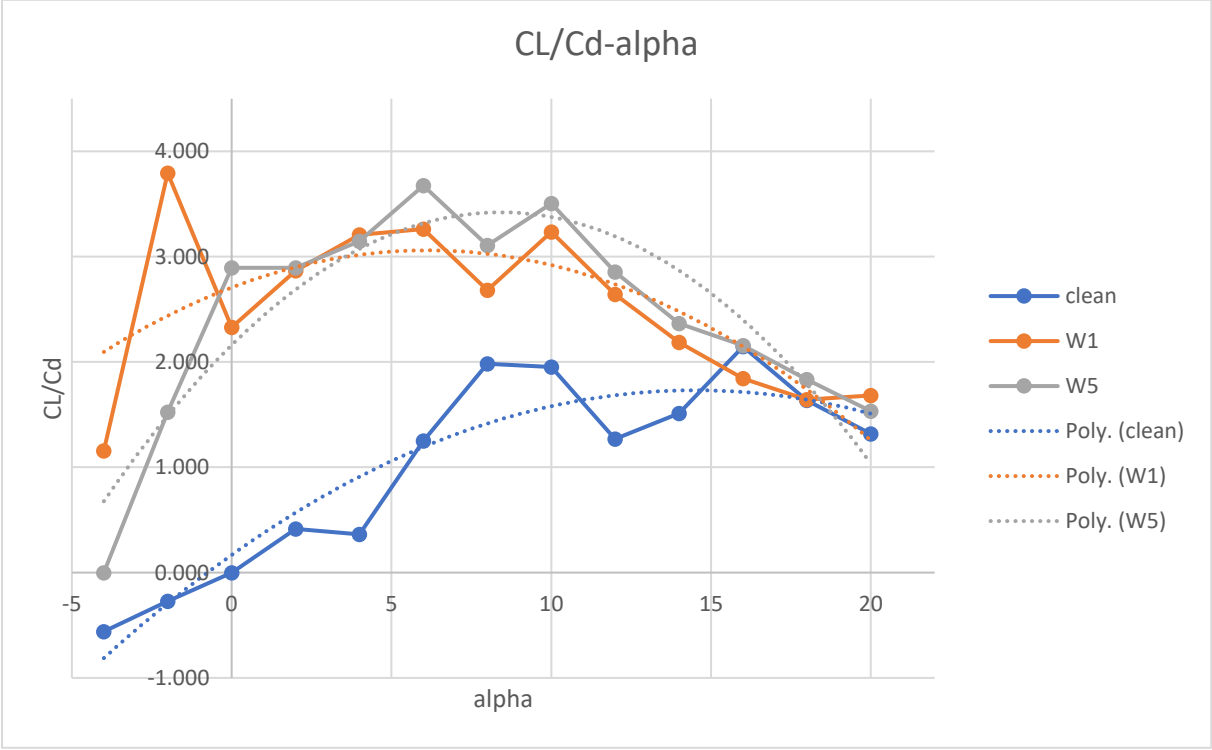

Figure 20-CL/Cd-alpha comparison

Each experiment's results are presented by using the gathered data from the experiment with the clean wing as a reference. It was expected from winglets added to the tip of the wing to increase the lift coefficient and, more importantly, decrease the drag coefficient of induced type.

Figure 18 compares the results of the lift coefficients for the three cases. A jump is detected in lift coefficients of the clean wing, and those two cases which have winglet and the winglets added to the wingtip in each case has increased the lift coefficient for about 0.14 in maximum. A notable result is that the two types of winglets affect the lift coefficient in the same manner and for about the same amounts.

Figure 19 compares the drag coefficient results. It was expected to find out a decrease in the drag coefficient by adding winglets at the wingtip. Still, results show that inserting a winglet at the tip of the wing increases the drag coefficient, and as can be seen in the results, the one-sided type of winglet increased the drag coefficient more than the double-sided type. The expected decrease in drag coefficient is predicted for the induced part of the drag coefficient based on the fluid's aerodynamic behavior at the tip of the wing, and this result may be found out by separating the types of drag forces that must be done in further investigations. Also, the more increase of the drag coefficient resulted from the one-sided winglet compared to the double-sided one may be related to the nonsymmetric shape of the one-sided winglet and the symmetric shape of the double-sided one.

Figure 20 also gives an overall comparison for the ratio of the lift coefficient and the drag coefficient. It brings this result that there can be an angle with the maximum amount of lift to drag ratio for all cases of the test. It also is seen that winglets lag this angle of maximum lift to drag ratio to the clean wing, and again this lag is more for the nonsymmetric winglet than the symmetric one.

In conclusion, adding winglets at the tip of a wing increases the lift coefficient and increases the total drag coefficient. A wing with winglets reaches its maximum lift to drag ratio at lower angles of attack to a wing without winglets.

References

[1]. Richard L. Kline & Floyd F. Fogleman. Dec 19, 1972. Kline Fogleman Airfoil for Aircraft. The *United States Patent No: 3706430*.

[2]. Richard L. Kline & Floyd F. Fogleman. Sept 6, 1977. Airfoil for Aircraft having Improved Lift Generating Device. The *United States Patent No: 4046338.*

[3]. FathiFinaish and Stephen Witherspoon. January 1998. Aerodynamic Performance of an Airfoil with Step-Induced Vortex for Lift Augmentation. The *University of Missouri*.

[4]. Adam Joseph Wells. 2005. Experimental Investigation of an Airfoil with COFLOWJET Flow Control. The *University of Florida*.

[5]. William S Johnson's paper on "Investigation of the Kline-Fogleman Airfoil Section for Rotor Blade Applications."

[6]. Mohammed Ahmed Rasheed & Ahmed Adnan AL-Qaisy. 2008. Experimental Investigation of Aerodynamic Characteristics of NACA 23015 under different angles of attack and Comparison with Available Package. *Mechanical Engineering Department. The University of Technology Baghdad*.

[7]. MILNE-THOMSON. L.M.," TheoreticalAerodynamics" Emeritus Professor of Applied Mathematics, University of Arizona, Emeritus Professor of Applied Mathematics in the Naval College, Professor of Applied Mathematics in Brown University, Emeritus Professor of Applied Mathematics Research Centre at the University of Wisconsin Visiting Professor at the Universities of Rome, Queensland, Calgary, Otago.

[8]. HANSEN. R. JAMES. D.BRYAN TAYLOR, JEREMY KINNEY, and J. LAWRENCE LEE, "The wind and Beyond," National Aeronautical and Space Administration, Washington, D.C.

[9]. L.J CLANCY. Aerodynamics for students.

[10]. JOHN D. ANDERSON JR. Fundamentals of Aerodynamics.

[11]. Jacobs, Eastman N., Ward, Kenneth E., and Pinkerton, Robert M.: The Characteristics of 78 Related Airfoil Sections from Tests in the Variable~Density Wind Tunnel. NACA Rep. No. 460, 1933.

[12]. Jacobs, Eastman N., and Pinkerton, Robert M.: Tests in the Variable-Density Wind Tunnel of Related Airfoils Having the Maximum Camber Unusually Far Forward. NACA Rep. No. 537, 1935. _

[13]. Jacobs, Eastman N., Pinkerton, Robert M., and Greenberg, Harry: Tests of Related Forward-Camber Airfoils in the Variable-Density Wind Tunnel. NACA Rep. No. 610, 1937.

[14]. Stack, John, and Von Doenhoff, Albert E.: Tests of 16 Related Airfoils' at High Speeds. NACA Rep. No. 492, 1934.

[15]. Jacobs, Eastman N., and Sherman, Albert: Airfoil Section Characteristics as Affected by Variations of the Reynolds Number. NACA Rep. No. 586, 1937.

[16]. Pinkerton, Robert M., and Greenberg, Harry: Aerodynamic Characteristics of a Large Number of Airfoils Tested in the Variable-Density Wind Tunnel. NACA Rep. No. 628, 1938.

[17]. Jones, B. Melvill: Flight Experiments on the Boundary Layer. _ Jour. Aero. Sci., vol. 5, no. 3, Jan. 1938, pp. 81-94.

[18]. Jacobs, Eastman N., and Abbott, Ira H.: Airfoil Section Data Obtained in the N.A.C.A. Variable-Density Tunnel as Affected by Support Interference and Other Corrections. NACA Rep. No. 669, 1939.

[19]. Theodorsen, Theodore: Theory of Wing Sections of Arbitrary Shape. NACA Rep. No. 411, 1931.

[20]. Stack, John: Tests of Airfoils Designed to Delay the Compressibility Burble. NACA Rep. No. 763, 1943.
[21]. Jacobs, Eastman N.: Preliminary Report on Laminar-Flow Airfoils and Jirew Methods Adopted for Airfoil and Boundary-Layer Investigations. NACA ACR June 1939.
[22]. Abbott, I.H., von Doenhoff, A.E., and Stivers, L.S., "Summary of Airfoil Data." NACA Report no. 824, 1945

[23]. Timmer, W.A., "An overview of NACA 6-digit airfoil series characteristics regarding airfoils for large wind turbine blades". ,2009

[24]. Loftin, L. K., and Poteat, M. I., "Aerodynamic characteristics of several NACA airfoils sections at seven Reynolds from 0.7*10^6 to 9.0*10^6

[25]. Abbott, Ira H., von Doenhoff, Albert E., and Stivers, Louis S., Jr.: "Summary of Airfoil Data." NACA ACR No. L5C05, 1945.

[26]. Module 08, Basic Aerodynamics, Part 66 courseware.

[27]. J. Anderson, "Fundamentals of Aerodynamics."